
Training Dense Object Nets: A Novel Approach

Anonymous Author(s)

Affiliation
Address
email

Abstract

Our work proposes a novel framework that addresses the computational resource limitations associated with training Dense Object Nets (DON) while achieving robust and dense visual object descriptors. DON’s descriptors are known for their robustness to viewpoint and configuration changes, but training them requires computationally expensive image pairs with correspondence mapping. This limitation hampers dimensionality and robustness, thereby restricting object generalization. To overcome this, we introduce a synthetic augmentation data generation procedure and a novel deep learning architecture that produces denser visual descriptors with reduced computational demands. Notably, our framework eliminates the need for image-pair correspondence mapping and showcases its application in a robot-grasping pipeline. Experimental results demonstrate that our approach yields descriptors as robust as those generated by DON.

1 Introduction

The objectives of long-standing robotics and robotic manipulation are to create a general-purpose robot capable of carrying out practical activities like Chappie [1] or C-3PO [2]. While advancements have been made recently in adjacent domains, achieving this goal remains a work in progress. For instance, AlphaGo [3], a game-playing artificial intelligence system trained entirely on self-play, defeated the world’s best human Go player at the time. Subsequently, Silver et al. [4] developed artificial intelligence algorithms that mastered the game of chess, Go, World of Warcraft [5], and Shogi, surpassing human playing expertise. Most of these algorithms learn directly from visual data, such as gameplay recordings or online video streams, emphasizing the importance of visual data in AI. Meanwhile, the launch of AlexNet [6] in 2012 transformed the field of computer vision. Other visual tasks, such as semantic segmentation [7], object identification and recognition [8], and human pose estimation [9], have also witnessed significant gains in recent years. Significant breakthroughs have been made in robotics, ranging from self-driving cars to humanoid robots capable of performing complex tasks using cameras and other vision sensors. Despite these advancements, the most frequently used robotic manipulation systems have evolved slightly in the previous 30 years. Typical auto-factory robots continue to perform repetitive operations such as welding and painting, following a pre-programmed course with no feedback from the surroundings. If we want to increase the utility of our robots, we must move away from highly controlled settings and robots that perform repetitive actions with little feedback or adaptability capabilities. Liberating ourselves from these constraints of controlled settings-based manufacturing would allow us to enter new markets, as witnessed by the proliferation of firms [10] competing in the logistics domain.

The ideal object representation for robot grasping and manipulation tasks remains to be engineered today. Existing representations may not be suitable for complex tasks due to limited capabilities of understanding an object’s geometrical and structural information. In 2018, Florence et al. [11] introduced a novel visual object representation to the robotics community, terming it “dense visual object descriptors”. DON, an artificial intelligence framework proposed by Florence et al. [11]

39 produces dense visual object descriptors. In detail, the DON converts every pixel in the image
 40 ($I[u, v] \in \mathbb{R}^3$) to a higher dimensional embedding ($I_D[u, v] \in \mathbb{R}^D$) such that $D \in \mathbb{N}^+$ consuming
 41 image-pair correspondences as input yielding pixelwise embeddings which are nothing but dense
 42 local descriptors. The dense visual object descriptor generalizes an object up to a certain extent
 43 and has been recently applied to rope manipulation [12], block manipulation [13], robot control
 44 [14], fabric manipulation [15] and robot grasp pose estimation [16, 17]. Adrian et al. [17] further
 45 demonstrated that DON can be trained on synthetic data and still generalize to real-world objects.
 46 Furthermore, Adrian et al. [17] demonstrated that the quality of descriptors produced by the DON
 47 framework depends on the higher or longer embedding dimension. We tried training the DON on
 48 a computation device equipped with NVIDIA RTX A6000 GPU with 48GB VRAM. However, we
 49 could not train the DON to produce a higher embedding dimension due to the limited VRAM. The
 50 DON framework is computationally expensive, as shown in Table 1, and limits the user to generalize
 51 objects to a certain extent making it difficult to use as a robot grasping pipeline in real-world logistics
 52 and warehouse automation scenarios.

Table 1: Benchmark of DON framework trained on GPU with 48GB VRAM with 128 image-pair correspondences, batch size of 1 and “Pixelwise NTXENT Loss” [17] as a loss function.

GPU VRAM consumption to train DON				
Descriptor Dimension	3	8	16	32
VRAM Usage (GB)	9.377	13.717	20.479	30.067

53 Moreover, today’s Large Language Models (LLMs) consume vast computational resources, posing
 54 significant concerns for the future. LLMs’ sheer size and complexity require massive computing
 55 power, leading to excessive energy consumption and environmental harm. Researchers and experts
 56 have raised alarm about these issues. As Bender et al. [18] highlighted, the environmental impact
 57 of training and operating LLMs at scale is substantial, contributing to increased carbon emissions.
 58 Furthermore, in their paper, Strubell et al. [19] emphasized how the resource-intensive nature of
 59 LLMs exacerbates the digital divide, limiting access to advanced AI technologies for underprivileged
 60 populations. The ethical implications of prioritizing computational power for LLMs over binding
 61 domains have also been acknowledged by researchers such as Amodei et al. [20], stressing the
 62 need for responsible resource allocation. Striking a balance between technological progress and
 63 sustainability is essential, as echoed by various experts in the field. Drawing motivation from LLMs
 64 impact of consumption of vast computational resources, we propose a novel framework to train and
 65 extract dense visual object descriptors produced by DON, which is computationally efficient.¹

66 2 Related Work

67 We are solely interested in computing dense visual object descriptors of an object. The DON training
 68 strategy in [11] relies on the depth information for computing correspondences in an image pair
 69 using camera intrinsics and pose information [21]. However, when employing consumer-grade depth
 70 cameras for capturing the depth information, the depth cameras capture noisy depth in cases of
 71 tiny, reflecting objects, which are common in industrial environments. In the meantime, Kupcsik
 72 et al. [16] used Laplacian Eigenmaps [22] to embed a 3D object model into an optimally generated
 73 embedding space acting as a target to train DON in a supervised fashion. The optimal embeddings
 74 bring more domain knowledge by associating the 3D object model with image views. Kupcsik
 75 et al. [16] efficiently apply it to smaller, texture-less and reflective objects by eliminating the need for
 76 depth information. Kupcsik et al. [16] further, compare training strategies for producing 6D grasps
 77 for industrial objects and show that a unique supervised training approach increases pick-and-place
 78 resilience in industry-relevant tasks.

79 Florence [23] has found that the pixelwise contrastive loss function used to train DON might not
 80 perform well if a computed correspondence is spatially inconsistent (analogously to the case of noisy
 81 depth information). Further highlighting that the precision of contrastive-trained models can be sensi-
 82 tive to the relative weighting between positive-negative sampled pixels. Instead, the Florence [23]
 83 introduces a new continuous sampling-based loss function called “Pixelwise Distribution Loss”. The

¹Dataset and codebase link: https://github.com/KanishkNavale/training_don_while_not_training_don

84 pixelwise distribution loss is much more effective as it is a smooth continuous pixel space sampling
 85 method compared to the discrete pixel space sampling method based on pixelwise contrastive loss.
 86 The pixelwise distribution loss regresses probability distribution heatmaps to minimize the divergence
 87 between the predicted heatmap and the ground truth heatmap mitigating errors in correspondences.
 88 Furthermore, the pixelwise distribution loss does not need non-matching correspondences com-
 89 pared to the pixelwise contrastive loss. Differently, Hadjivelichkov and Kanoulas [24] extends the
 90 DON training using semantic correspondences between objects in multi-object or cluttered scenes
 91 overcoming the limitations of [21, 22]. The authors, Hadjivelichkov and Kanoulas [24] employ
 92 offline unsupervised clustering based on confidence in object similarities to generate hard and soft
 93 correspondence labels. The computed hard and soft labels lead DON in learning class-aware dense
 94 object descriptors, introducing hard and soft margin constraints in the proposed pixelwise contrastive
 95 loss to train DON. Further eliminating the need for camera pose and intrinsic information along
 96 with depth information to compute correspondences in an image pair, Yen-Chen et al. [25] used
 97 NeRF [26] to train DON. The NeRF [26] recreates a 3D scene from a sequence of images captured
 98 by the smartphone camera. The correspondences are extracted from the synthetically reconstructed
 99 scene to train DON. Recently, based on SIMCLR inspired frameworks [27, 28], Adrian et al. [17]
 100 introduced similar architecture and another novel loss function called Pixelwise NTXent loss to train
 101 DON more robustly. The Pixelwise NTXent loss consumes synthetic correspondences independent of
 102 depth cameras computed from image augmentations to train DON. Adrian et al.’s experiments show
 103 that the novel loss function is invariant to the batch size. Additionally adopted “*PCK@k*” metric
 104 has been adopted as in proceedings [29, 30] to evaluate and benchmark DON on cluttered scenes
 105 previously not benchmarked.

106 In the proposed framework, we do not use any loss functions in [11, 23, 16, 17, 24, 25] to train DON
 107 however we adopt the network architecture from [11] and train on the task of the KeypointNet[31,
 108 32].

109 3 Methodology

110 3.1 Dataset Engineering

111 We have chosen the cap object for creating a synthetic dataset as the cap mesh models are readily
 112 available in the “Shapenet” library [33] as it contains rich object information, including textures.
 113 Furthermore, we choose five cap models from the Shapenet library and use Blenderproc [34] to
 114 generate the synthetic dataset. For each cap model, we save one RGB image, mask and depth
 115 from the synthetic scene. Additionally, we employ synthetic augmentations as proposed in [17]
 116 to synthetically spatial augment the cap’s position and rotation in an image, including background
 117 randomization using Torchvision [35] library. To generate camera poses for different viewpoints, an
 118 augmented image-pair is sampled randomly, additionally image-pair correspondences are computed¹
 119 as illustrated in the Figure 1. Using depth information, we project the computed correspondences to
 120 the camera frame and compute the relative transformation between two camera-frame coordinates of
 121 the correspondences using Kabsch’s transformation [36].

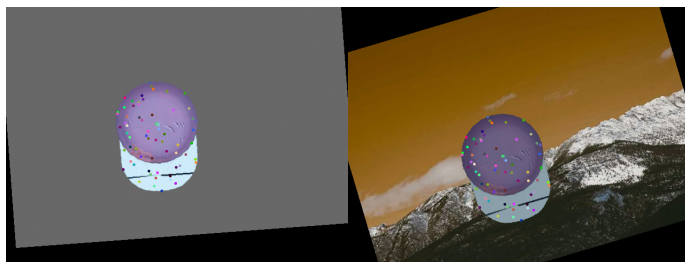


Figure 1: Depiction of image synthetic spatial augmentation and correspondences mapping in an image-pair. The colored encoded dots in the figure represents correspondences in an image-pair.

¹GitHub Link:
<https://github.com/KanishkNavale/Mapping-Synthetic-Correspondences-in-an-Image-Pair>

122 **3.2 Framework & Mining Strategy**

123 As a backbone, we employ ResNet-34 architecture [37]. We preserve the last convolution layer and
 124 remove the pooling and linear layers. The backbone downsamples the RGB image $I_{RGB} \in \mathbb{R}^{H \times W \times 3}$
 125 to dense features $I_d \in \mathbb{R}^{h \times w \times D}$ such that $h \ll H, w \ll W$ and $D \in \mathbb{N}^+$. We upsample the dense
 126 features from the identity layer (being identical to the last convolution layer in the backbone) as
 127 illustrated in the Figure 2 in page 4 as follows:

$$f_U : I \in \mathbb{R}^{h \times w \times D} \rightarrow I_D \in \mathbb{R}^{H \times W \times D}. \quad (1)$$

128 The upsampled dense features are extracted and treated as dense visual local descriptors produced
 129 from the DON. In otherwords we extract or mine the representations from the backbone. Similarly as
 130 in [31], we stack spatial-probability regressing layer and depth regressing layer on top of the identity
 131 layer to predict $N \in \mathbb{N}^+$ number of keypoint's spatial-probability as follows:

$$f_S : I_d \in \mathbb{R}^{h \times w \times D} \rightarrow I_s^N \in \mathbb{R}^{h \times w \times N}, \quad (2)$$

132 and depth as follows:

$$f_D : I_d \in \mathbb{R}^{h \times w \times D} \rightarrow I_{\hat{d}} \in \mathbb{R}^{h \times w \times N}. \quad (3)$$

133 We incorporate continuous sampling method f_E from [23, 31] to convert the upsampled predicted
 134 spatial-probability and depth of a keypoint to spatial-depth expectation as follows:

$$f_E \circ g_E : [I_s, I_{\hat{d}}] \rightarrow [u, v, d]^T \in \mathbb{R}^3, \text{ where } g_E : I \in \mathbb{R}^{h \times w \times N} \rightarrow I \in \mathbb{R}^{H \times W \times N}. \quad (4)$$

135 Furthermore, we train the framework in a twin architecture fashion as proposed in [27, 28, 11, 23, 16,
 136 17, 24, 25] on the modified KeypointNet task.

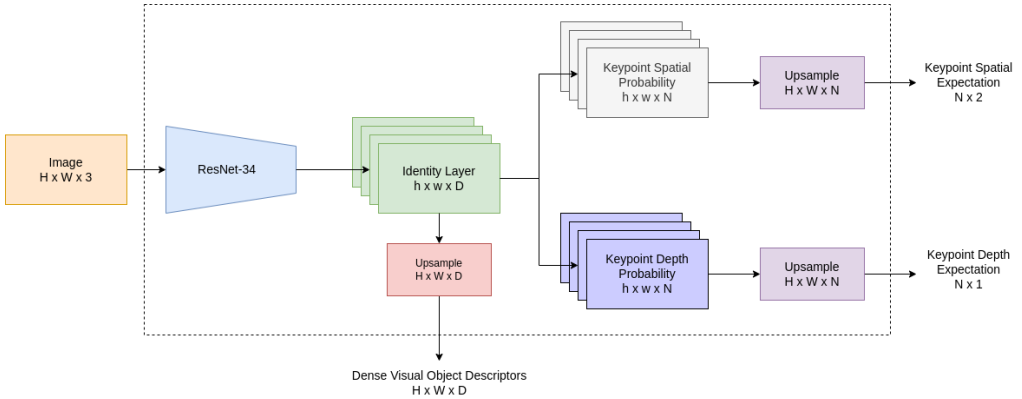


Figure 2: Illustration of the novel framework designed to compute and seamlessly extract dense visual object descriptors efficiently. During inference, we extract dense visual object descriptors directly from the network and ignore predicted spatial-depth expectations of the keypoints.

137 **3.3 Loss Functions**

138 For training, we directly adopt silhouette consistency loss (\mathcal{L}_{obj}), variance loss (\mathcal{L}_{var}) and separation
 139 loss (\mathcal{L}_{sep}) functions from [31] to train the network on the keypoint prediction task. However, we
 140 modify the multi-view consistent loss and relative pose estimation loss. In the case of multi-view
 141 consistency loss we project the predicted spatial-depth expectation using camera intrinsics as follows:
 142

$$X_{cam} \in \mathbb{R}^{3 \times 1} = \mathcal{I}_{cam}^{-1} [u, v, 1.0]^T \times d, \text{ where } \mathcal{I}_{cam} \in \mathbb{R}^{3 \times 3} \text{ and } u, v, d \in \mathbb{R}^+. \quad (5)$$

143 Furthermore, we project the camera coordinates of the keypoints from one camera viewpoint to
 144 another camera viewpoint using relative transformation supplied from the synthetic augmentation
 145 procedure as follows:

$$\mathcal{L}_{mvc} \in \mathbb{R} = \mathcal{H}(\hat{X}_{cam}^B, \mathcal{T}_{A \rightarrow B} \hat{X}_{cam}^A), \text{ where } \hat{X}_{cam} = [X_{cam}, 1.0]^T \in \mathbb{R}^{4 \times 1}, \quad (6)$$

146 In Equation 6, $\mathcal{T}_{A \rightarrow B} \in SE(3)$ is a Special Euclidean Group [38] which is relative transformation
 147 from camera-frame A to camera-frame B . We use Huber loss \mathcal{H} as it produces smoother gradients
 148 for framework optimization. Furthermore, we do not discard the relative transformation information
 149 to calculate the relative pose loss as suggested in [31]. Moreover, being influenced from [32] we
 150 modified the relative pose loss as follows:

$$\mathcal{L}_{pose} = \|log(\mathcal{T}_{truth}^\dagger \mathcal{T}_{pred})\|, \text{ where } log : SE(3) \rightarrow \mathfrak{se}(3) \text{ and } \mathcal{T}^\dagger = \begin{bmatrix} R^T & -R^T t \\ 0^T & 1 \end{bmatrix}. \quad (7)$$

151 3.4 Robot Grasping Pipeline

152 To use the proposed framework as a robot grasping pipeline, we extract dense visual object descriptors
 153 from the network and store one single descriptor of objects in a database manually for now. During
 154 inference, we extract dense visual object descriptors from the network and query the descriptor from
 155 the database to find the closest match as follows:

$$\mathbb{E}[u^*, v^*]_d = \underset{u, v}{\operatorname{argmin}} \exp - \left(\frac{\|I_D[u, v] - d\|}{\exp(t)} \right)^2, \text{ where } \|I_D[u, v] - d\| \in \mathbb{R}^{H \times W}. \quad (8)$$

156 Where $t \in \mathbb{R}$ controls the kernel width influencing the search space to compute the optimal spatial
 157 expectation $\mathbb{E}[u^*, v^*]_d$ of the query descriptor $d \in \mathbb{R}^D$ in the descriptor image $I_D \in \mathbb{R}^{H \times W \times D}$.
 158 The computed spatial expectation is projected to the robot frame using camera intrinsics and poses
 159 to perform a pinch grasp. Furthermore, the Franka Emika 7-DOF robot manipulator with two jaw
 160 gripper and wrist-mounted Intel Realsense D435 camera is used as a testing setup as illustrated in
 161 Figure 3.



Figure 3: Illustration of the robot grasping pipeline setup. In the image, the robot is highlighted in red, the caps in green, and the camera in blue.

162 4 Experiments & Results

163 4.1 Dense Object Nets

164 We implemented training and benchmarking using “PyTorch-Lightning”[39] and “PyTorch”[40]
 165 libraries. Furthermore, we employ ADAM[41] optimizer to optimize the model for 2500 epochs
 166 with a learning rate of $\alpha = 3 \times 10^{-4}$, $\beta_1 = 0.9$ and $\beta_2 = 0.999$ with weight decay $\eta = 10^{-4}$ to
 167 benchmark the DON with Pixelwise NT-Xent loss as in [17] with a fixed batch size of 1 and 128
 168 image-pair correspondences. As per the benchmarking results in Table 2, the descriptor’s robustness
 169 increases as the descriptor’s dimension gets longer.

Table 2: Benchmark of DON framework for GPU consumption and $AUC \pm \sigma$ for $PCK@k$, $\forall k \in [1, 100]$ metric.

DON benchmark				
Descriptor Size (D)	3	8	4	32
AUC for $PCK@k$	0.922 ± 0.006	0.933 ± 0.011	0.948 ± 0.012	0.953 ± 0.008
VRAM Usage (GB)	9.377	13.717	20.479	30.067

170 The $AUC \pm \sigma$ for $PCK@k, \forall k \in [1, 100]$ is computed with 256 image-pair correspondences and
 171 the metrics mean and std. deviation is calculated from benchmarking 3 DON models trained for a
 172 single descriptor dimension. We could not train the descriptor dimension of 64 and 128 due to the
 173 limited VRAM. Furthermore, to inspect the results of trained DON, an interface is built using the
 174 PyGame library [42] to visualize the results of the trained DON. The mouse pointer in the image
 175 space is mapped to the pixel, and the descriptor at that pixel is queried in another image-descriptor
 176 space. We further use the spatial probability of the descriptor to visualize the queried descriptor
 177 in the image space using Equation 8 Identify if there are any multi-modal spatial activations in the
 178 descriptor spaces and none, as shown in Figure 4.



Figure 4: Depiction of the spatial probability heatmaps of the descriptor in the image space. We set the temperature in the Equation 8 to 1.1 and render the spatial probability heatmaps in the interface. The first and second image from the left and the right highlights the semantically equivalent descriptors in the image space.

179 4.2 Our Framework

180 To train our framework, we employ an ADAM optimizer to optimize the model for 2500 epochs with
 181 a learning rate of $\alpha = 1 \times 10^{-3}$, $\beta_1 = 0.9$ and $\beta_2 = 0.999$ with no weight decay. We further use a
 182 fixed batch size of 1 and the StepLR scheduler with a step size 2500 and a gamma of 0.9 to train the
 183 model with all the loss weights to 1.0 except variance loss weight to 1×10^{-3} . At first, we trained
 184 our model with 16 keypoints with a margin of 10 pixels as a hyperparameter for the separation loss,
 185 and later, we trained the models with 128 keypoints with a margin of 2 pixels.

Table 3: Benchmark of our framework for GPU consumption and $AUC \pm \sigma$ for $PCK@k, \forall k \in [1, 100]$ metric.

Our framework with 16 keypoints				
Descriptor Size (D)	64	128	256	512
$AUC \pm \sigma$ for $PCK@k$	0.922 ± 0.006	0.933 ± 0.011	0.948 ± 0.012	0.953 ± 0.008
VRAM Usage (GB)	3.799	4.191	5.241	7.341
Our framework with 128 keypoints				
Descriptor Size (D)	64	128	256	512
$AUC \pm \sigma$ for $PCK@k$	0.922 ± 0.006	0.933 ± 0.011	0.948 ± 0.012	0.953 ± 0.008
VRAM Usage (GB)	4.913	5.409	6.551	7.915

186 4.3 Robot Grasping Pipeline

187 For the robot grasping pipeline, we trained our framework with actual caps. As the synthetic data
 188 generation only needs mask and depth information, we could create a mask in no time. Additionally,
 189 while training the framework, we do not need the actual real-world depth information as it computes
 190 its own. We later extracted the dense visual local descriptors from the framework. We visually
 191 inspected for any inconsistencies in the descriptor space, as shown in Figure 5, and found it consistent.
 192 Furthermore, we did not use the models trained on the synthetic dataset, as the representations were
 193 inconsistent with the real caps.

194 For robot grasping, a descriptor is picked from the descriptor space and queried in real-time such that
 195 robot can pinch-grasp the object. We could successfully grasp the caps with the robot, as shown in
 196 Figure 6.

197 As our framework inertly regresses keypoints on the object, we could use it as an alternative approach
 198 to grasp the caps by computing the pose generated by the keypoints considering the actual depth

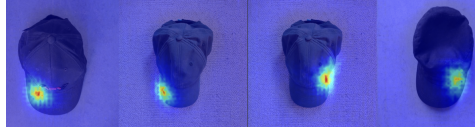


Figure 5: Visual inspection of the dense visual descriptors space of the real caps.

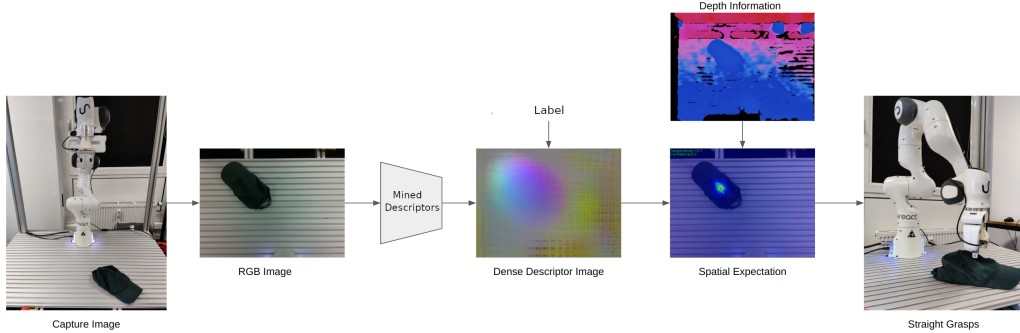


Figure 6: Depiction of the straight robot grasping pipeline.

199 information instead of network-regressed depth information. We extract the spatial probability of
 200 each keypoint from the framework and deactivate spatial probabilities where the depth information is
 201 missing, as the depth image from the camera is noisy. Furthermore, the spatial expectations of the
 202 keypoints are projected to the camera frame to calculate a 6D pose in the camera frame. The 6D pose
 203 is transformed in the robot frame to perform an aligned grasp, as shown in Figure 7.

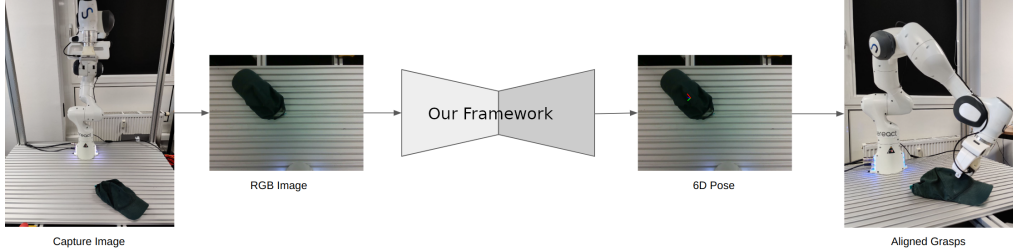


Figure 7: Illustration of the aligned robot grasping pipeline.

204 We did not evaluate the robot grasping pipeline.

205 **5 Conclusion**

206 We present a novel framework for mining dense visual object descriptors without explicitly training
 207 DON. By leveraging synthetic augmentation data generation and a novel deep learning architecture,
 208 our approach produces robust and denser visual local descriptors while consuming up to 86.67%
 209 lesser computational resources than the originally proposed framework. Furthermore, it eliminates
 210 the additional task of computing a large number of image-pair correspondences. We demonstrate the
 211 application of our framework as a robot-grasping pipeline in two methodologies, one of which our
 212 framework demonstrates its capabilities to produce object-specific 6D poses for robot grasping.

213 **6 Future Work**

214 The framework will be extended to produce multi-object dense visual descriptors in cluttered scenes.
 215 Furthermore, we will start incorporating ROI layers in the framework and adding additional object
 216 classification loss functions.

217 **References**

- 218 [1] N. Blomkamp, H. Zimmer, and S. Kinberg. *Chappie*. Sony Pictures Home Entertainment, 2015.
- 219 [2] G. Lucas and S. Ulstein. *Star wars*. 20th Century-Fox, 1977.
- 220 [3] D. Silver, T. Hubert, J. Schrittwieser, I. Antonoglou, M. Lai, A. Guez, M. Lanctot, L. Sifre, D. Kumaran, T. Graepel, et al. “A general reinforcement learning algorithm that masters chess, shogi, and Go through self-play”. In: *Science* 362.6419 (2018), pp. 1140–1144.
- 223 [4] D. Silver, A. Huang, C. J. Maddison, A. Guez, L. Sifre, G. Van Den Driessche, J. Schrittwieser, I. Antonoglou, V. Panneershelvam, M. Lanctot, et al. “Mastering the game of Go with deep neural networks and tree search”. In: *nature* 529.7587 (2016), pp. 484–489.
- 226 [5] B. Entertainment. *World of warcraft*. Insight Editions, Division Of Palac, 2013.
- 227 [6] A. Krizhevsky, I. Sutskever, and G. E. Hinton. “Imagenet classification with deep convolutional neural networks”. In: *Communications of the ACM* 60.6 (2017), pp. 84–90.
- 229 [7] J. Long, E. Shelhamer, and T. Darrell. “Fully convolutional networks for semantic segmentation”. In: *Proceedings of the IEEE conference on computer vision and pattern recognition*. 2015, pp. 3431–3440.
- 231 [8] K. He, G. Gkioxari, P. Dollár, and R. Girshick. “Mask r-cnn”. In: *Proceedings of the IEEE international conference on computer vision*. 2017, pp. 2961–2969.
- 233 [9] R. A. Güler, N. Neverova, and I. Kokkinos. “Densepose: Dense human pose estimation in the wild”. In: *Proceedings of the IEEE conference on computer vision and pattern recognition*. 2018, pp. 7297–7306.
- 235 [10] sereact. “AI Robots for Production. Today”. <https://sereact.ai/en>.
- 236 [11] P. R. Florence, L. Manuelli, and R. Tedrake. “Dense object nets: Learning dense visual object descriptors by and for robotic manipulation”. In: *arXiv preprint arXiv:1806.08756* (2018).
- 238 [12] P. Sundaresan, J. Grannen, B. Thananjeyan, A. Balakrishna, M. Laskey, K. Stone, J. E. Gonzalez, and K. Goldberg. “Learning Rope Manipulation Policies Using Dense Object Descriptors Trained on Synthetic Depth Data”. In: *CoRR* abs/2003.01835 (2020). arXiv: 2003.01835.
- 241 [13] C.-Y. Chai, K.-F. Hsu, and S.-L. Tsao. “Multi-step Pick-and-Place Tasks Using Object-centric Dense Correspondences”. In: *2019 IEEE/RSJ International Conference on Intelligent Robots and Systems (IROS)*. 2019, pp. 4004–4011. DOI: 10.1109/IROS40897.2019.8968294.
- 244 [14] P. Florence, L. Manuelli, and R. Tedrake. “Self-supervised correspondence in visuomotor policy learning”. In: *IEEE Robotics and Automation Letters* 5.2 (2019), pp. 492–499.
- 246 [15] A. Ganapathi et al. “Learning Dense Visual Correspondences in Simulation to Smooth and Fold Real Fabrics”. In: *2021 IEEE International Conference on Robotics and Automation (ICRA)*. 2021, pp. 11515–11522. DOI: 10.1109/ICRA48506.2021.9561980.
- 249 [16] A. Kupcsik, M. Spies, A. Klein, M. Todescato, N. Wanek, P. Schillinger, and M. Bürger. “Supervised Training of Dense Object Nets using Optimal Descriptors for Industrial Robotic Applications”. In: *arXiv preprint arXiv:2102.08096* (2021).
- 252 [17] D. B. Adrian, A. G. Kupcsik, M. Spies, and H. Neumann. “Efficient and Robust Training of Dense Object Nets for Multi-Object Robot Manipulation”. In: *2022 International Conference on Robotics and Automation (ICRA)*. IEEE. 2022, pp. 1562–1568.
- 255 [18] E. M. Bender, T. Gebru, A. McMillan-Major, and S. Shmitchell. “On the Dangers of Stochastic Parrots: Can Language Models Be Too Big?” In: *Proceedings of the 2021 ACM conference on fairness, accountability, and transparency*. 2021, pp. 610–623.
- 258 [19] E. Strubell, A. Ganesh, and A. McCallum. “Energy and policy considerations for deep learning in NLP”. In: *arXiv preprint arXiv:1906.02243* (2019).
- 260 [20] D. Amodei, C. Olah, J. Steinhardt, P. Christiano, J. Schulman, and D. Mané. “Concrete problems in AI safety”. In: *arXiv preprint arXiv:1606.06565* (2016).
- 262 [21] R. Hartley and A. Zisserman. *Multiple view geometry in computer vision*. Cambridge university press, 2003.
- 264 [22] M. Belkin and P. Niyogi. “Laplacian eigenmaps for dimensionality reduction and data representation”. In: *Neural computation* 15.6 (2003), pp. 1373–1396.
- 266 [23] P. R. Florence. “Dense visual learning for robot manipulation”. PhD thesis. Massachusetts Institute of Technology, 2020.
- 268 [24] D. Hadjiveliadis and D. Kanoulas. “Fully Self-Supervised Class Awareness in Dense Object Descriptors”. In: *5th Annual Conference on Robot Learning*. 2021.
- 270 [25] L. Yen-Chen, P. Florence, J. T. Barron, T.-Y. Lin, A. Rodriguez, and P. Isola. *NeRF-Supervision: Learning Dense Object Descriptors from Neural Radiance Fields*. 2022. DOI: 10.48550/ARXIV.2203.01913.
- 272 [26] B. Mildenhall, P. P. Srinivasan, M. Tancik, J. T. Barron, R. Ramamoorthi, and R. Ng. “Nerf: Representing scenes as neural radiance fields for view synthesis”. In: *Communications of the ACM* 65.1 (2021), pp. 99–106.

- 275 [27] T. Chen, S. Kornblith, M. Norouzi, and G. Hinton. “A simple framework for contrastive learning of visual
276 representations”. In: *International conference on machine learning*. PMLR. 2020, pp. 1597–1607.
- 277 [28] J. Zbontar, L. Jing, I. Misra, Y. LeCun, and S. Deny. “Barlow twins: Self-supervised learning via
278 redundancy reduction”. In: *International Conference on Machine Learning*. PMLR. 2021, pp. 12310–
279 12320.
- 280 [29] C.-Y. Chai, K.-F. Hsu, and S.-L. Tsao. “Multi-step pick-and-place tasks using object-centric dense
281 correspondences”. In: *2019 IEEE/RSJ International Conference on Intelligent Robots and Systems (IROS)*.
282 IEEE. 2019, pp. 4004–4011.
- 283 [30] M. E. Fathy, Q.-H. Tran, M. Z. Zia, P. Vernaza, and M. Chandraker. “Hierarchical metric learning and
284 matching for 2d and 3d geometric correspondences”. In: *Proceedings of the european conference on*
285 *computer vision (ECCV)*. 2018, pp. 803–819.
- 286 [31] S. Suwajanakorn, N. Snavely, J. J. Tompson, and M. Norouzi. “Discovery of latent 3d keypoints via
287 end-to-end geometric reasoning”. In: *Advances in neural information processing systems* 31 (2018).
- 288 [32] W. Zhao, S. Zhang, Z. Guan, W. Zhao, J. Peng, and J. Fan. “Learning deep network for detecting 3d
289 object keypoints and 6d poses”. In: *Proceedings of the IEEE/CVF Conference on computer vision and*
290 *pattern recognition*. 2020, pp. 14134–14142.
- 291 [33] A. X. Chang, T. Funkhouser, L. Guibas, P. Hanrahan, Q. Huang, Z. Li, S. Savarese, M. Savva, S. Song,
292 H. Su, et al. “Shapenet: An information-rich 3d model repository”. In: *arXiv preprint arXiv:1512.03012*
293 (2015).
- 294 [34] M. Denninger, M. Sundermeyer, D. Winkelbauer, Y. Zidan, D. Olefir, M. Elbadrawy, A. Lodhi, and
295 H. Katam. “Blenderproc”. In: *arXiv preprint arXiv:1911.01911* (2019).
- 296 [35] S. Marcel and Y. Rodriguez. “Torchvision the machine-vision package of torch”. In: *Proceedings of the*
297 *18th ACM international conference on Multimedia*. 2010, pp. 1485–1488.
- 298 [36] W. Kabsch. “A solution for the best rotation to relate two sets of vectors”. In: *Acta Crystallographica*
299 *Section A: Crystal Physics, Diffraction, Theoretical and General Crystallography* 32.5 (1976), pp. 922–
300 923.
- 301 [37] K. He, X. Zhang, S. Ren, and J. Sun. “Deep residual learning for image recognition”. In: (2016), pp. 770–
302 778.
- 303 [38] W. P. Thurston. “Three-Dimensional Geometry and Topology, Volume 1”. In: *Three-Dimensional Geome-*
304 *try and Topology, Volume 1*. Princeton university press, 2014.
- 305 [39] W. A. Falcon. “Pytorch lightning”. In: *GitHub* 3 (2019).
- 306 [40] A. Paszke, S. Gross, F. Massa, A. Lerer, J. Bradbury, G. Chanan, T. Killeen, Z. Lin, N. Gimelshein,
307 L. Antiga, et al. “Pytorch: An imperative style, high-performance deep learning library”. In: *Advances in*
308 *neural information processing systems* 32 (2019).
- 309 [41] D. P. Kingma and J. Ba. “Adam: A method for stochastic optimization”. In: *arXiv preprint*
310 *arXiv:1412.6980* (2014).
- 311 [42] S. Kelly. “Basic introduction to pygame”. In: *Python, PyGame and Raspberry Pi Game Development*.
312 Springer, 2016, pp. 59–65.